ROYAL SOCIETY OF CHEMISTRY

ARTICLE

Homoleptic complexes of a porphyrinatozinc(II)– 2,2':6',2''-terpyridine ligand

Angelo Lanzilotto,[a] Martin Kuss-Petermann,[b] Oliver S. Wenger,[b] Edwin C. Constable[a] and Catherine E. Housecroft*[a]

Three homoleptic complexes containing the metalloligand 7-(4-([2,2':6',2''-terpyridin]-4'-yl)phenyl)-5,10,15,20-tetraphenylporphyrinatozinc(II), **1**, have been prepared. $[Zn(\mathbf{1})_2][PF_6]_2$, $[Fe(\mathbf{1})_2][PF_6]_2$ and $[Ru(\mathbf{1})_2][PF_6]_2$ were characterized by ^1H and ^{13}C NMR spectroscopies and mass spectrometry, and the electrochemical and photophysical properties of the complexes have been investigated. In solution, each complex undergoes two, reversible porphyrin-centred oxidation processes, with an additional reversible metal-centred oxidation for $[Fe(\mathbf{1})_2][PF_6]_2$ and $[Ru(\mathbf{1})_2][PF_6]_2$. Solution absorption spectra are dominated by the Soret and Q bands of the metalloligand **1**. Spectroelectrochemical data for the complexes are presented. The results of a nanosecond transient absorption spectroscopic investigation of $[Zn(\mathbf{1})_2][PF_6]_2$, $[Fe(\mathbf{1})_2][PF_6]_2$ and $[Ru(\mathbf{1})_2][PF_6]_2$ are presented. For $[Zn(\mathbf{1})_2][PF_6]_2$, S_1 excitation leads to efficient intersystem-crossing to the T_1 state, whilst for $[Fe(\mathbf{1})_2][PF_6]_2$, excitation of the ^1MLCT transition is followed by fast deactivation to the ^3MC state followed by thermal decay to the ground state. Excitation of the ^1MLCT transition of $[Ru(\mathbf{1})_2][PF_6]_2$ results in an intersystem crossing to ^3MLCT; triplet-to-triplet energy transfer occurs giving the [Zn(TPP)] T_1 state which regenerates the ground state of the complex.

Introduction

The chemistry of oligopyridine-metalloporphyrin conjugates is a relatively underdeveloped field. Conjugates incorporating 2,2':6',2''-terpyridine (tpy) are attractive targets for the study of electron and energy-transfer processes and photosynthetic models.[1,2,3,4,5,6,7,8] Functionalization of porphyrin cores with 2,2'-bipyridine[9,10,11,12,13,14,15] or 1,10-phenanthroline[16,17] gives access to systems which can assemble heteroleptic tris(chelate) metal complexes, and a number of multinuclear arrays have been described incorporating pyridine-decorated porphyrins.[18,19,20,21,22] An alternative approach to assembly of metalloporphyrin-centred conjugates makes use of the axial coordination site of the metalloporphyrin, for example by the binding of metal complexes of 4'-(4-pyridyl)-2,2':6',2''-terpyridine.[23]

We recently reported a new strategy for the functionalization of porphyrins in which a tpy domain is attached to a pyrrole ring of the porphyrin core.[8] For synthetic reasons, functionalities are commonly introduced in the *meso*-positions of the porphyrin ring (5,10,15,20-substitution). However, by utilizing the selective monobromination of 5,10,15,20-tetraphenyl-21H,23H-porphyrin (H₂TPP) in one pyrrole ring reported by Zhang and coworkers, mono-functionalization of [ZnTPP] with a 4(4'-phenyl-2,2':6',2''-

terpyridyl) substituent is readily achieved.[8] Competition between the porphyrin and tpy units for metal ion coordination means that the porphyrin domain should be metallated before the porphyrin core is functionalized with the tpy domain. To date, we have only explored the formation of a single heteroleptic ruthenium(II) complex containing metalloligand **1** (Scheme 1) and we were therefore motivated to explore further the coordination chemistry of this new ligand, and to investigate how the inclusion of the peripheral metalloporphyrin units affect the electrochemical and spectroscopic properties of the complexes. We now present the synthesis and spectroscopic properties of a series of homoleptic complexes of the metalloligand **1**.

Experimental

General. ^1H and ^{13}C NMR spectra were recorded at room temperature using a Bruker Avance III-500 NMR spectrometer. ^1H and ^{13}C NMR chemical shifts were referenced to residual solvent peaks with respect to δ(TMS) = 0 ppm. Solution absorption spectra were measured using an Agilent 8453 spectrophotometer. Spectroelectrochemical and solid-state absorption spectroscopic measurements used a Varian-Cary 5000 spectrophotometer. MALDI-TOF and electrospray (ESI) mass spectra were recorded using Bruker Microflex and Bruker esquire 3000^{plus} instruments, respectively. Nanosecond

transient absorption spectra were measured on an LP-920KS spectrometer from Edinburgh Instruments using a frequency-doubled/tripled Quantel Brilliant B laser equipped with an OPO from Opotek as a pump source. The pulse duration was ~10 ns with an typical energy of 15 mJ. UV/Vis Transient absorption spectra were recorded with an iCCD camera from Andor. NIR transient absorption spectra were obtained from kinetic decays recorded with InGaAs photodiode.

Electrochemical measurements were made using a CH Instruments 900B potentiostat with $[^nBu_4N][PF_6]$ (0.1 M) as supporting electrolyte and at a scan rate of 0.1 V s^{-1}. The working electrode was glassy carbon, pseudo-reference J were referenced with respect to the Fc/Fc$^+$ couple. Spectroelectrochemical measurements were made with CH$_3$CN solutions of $[Zn(1)_2][PF_6]_2$ (0.09 M), $[Fe(1)_2][PF_6]_2$ (0.21 M), $[Ru(1)_2][PF_6]_2$ (0.04 M) at room temperature with $[^nBu_4N][PF_6]$ ($\approx$0.1 M) as the supporting electrolyte. The solution was added to an optically transparent thin-layer electrochemical (OTTLE) cell with two Pt minigrid electrodes (working and auxiliary), a silver wire pseudo-reference electrode and a path length of $\approx$0.2 mm. The potential was controlled using a VersaSTAT 3 potentiostat from Princeton Applied Research.

Compound **1** was prepared as previously described.[8] Details of $[Zn(ttpy)_2][PF_6]_2$ (ttpy = 4'-(4-tolyl-2,2':6',2''-terpyridine) used as a reference compound are given in the ESI†.

[Zn(1)$_2$][PF$_6$]$_2$. Compound **1** (53 mg, 0.054 mmol) and Zn(OAc)$_2$·2H$_2$O (6 mg, 0.027 mmol) were dissolved in dry MeOH (15 mL) under N$_2$ and the solution was stirred overnight at room temperature. An excess of saturated aqueous NH$_4$PF$_6$ was then added. A precipitate formed, which was collected by centrifuging. The solid was washed with water (3 × 5 mL) and Et$_2$O (3 × 5 mL), and then dissolved in MeCN; the solvent was removed under vacuum. $[Zn(1)_2][PF_6]_2$ was isolated as a dark-purple solid (56 mg, 0.024 mmol, 90%). ^{1}H NMR (500 MHz, (CD$_3$)$_2$CO) δ/ppm: 9.44 (s, 4H, H^{B3}), 9.22 (m, 4H, H^{A3}), 8.90 (d, J = 4.5 Hz, 2H, H$^{F3'/F4'}$), 8.88 (d, J = 4.5 Hz, 2H, H$^{F3'/F4'}$), 8.86 (s, 2H, H^{H3}), 8.86 (s, 4H, H^{I3+I4}), 8.82 (d, J = 4.6, 2H, H$^{F3/F4}$), 8.79 (d, J = 4.6, 2H, H$^{F3/F4}$), 8.41 (ddd, J = 8.1, 7.4, 1.6 Hz, 4H, H^{A4}), 8.31 (m, 8H, H^{A6+G2}), 8.24 (m, 8H, H$^{E2+E2'}$), 8.17-8.20 (m, 4H, H^{C2}), 8.04 (m, 4H, H^{D2}), 7.79-7.86 (m, 18H, H$^{E3+E3'+E4+E4'+G3+G4}$), 7.72 (m, 4H, H^{C3}), 7.66 (ddd, J = 7.4, 5.2, 1.0 Hz, 4H, H^{A5}), 7.36-7.44 (m, 6H, H^{D3+D4}). ^{13}C NMR (126 MHz, (CD$_3$)$_2$CO) δ/ppm: 156.6 (C^{B4}), 150.2 (C^{A2}), 151.0/150.5/150.2/147.4/146.0 (C$^{F2+F5+F2'+F5'+H2+H4+H5+I2+I5}$), 149.0 (C^{A6}), 148.4 (C^{B2}), 143.6 (C$^{C1+G1+E1+E1'}$), 142.3 (C^{D1}), 142.2 (C^{A4}), 136.7 (C^{D2}), 135.4 (C^{I3+I4}), 135.35 (C^{H3}), 135.1 (C$^{G2+E2+E2'}$), 133.8 (C^{C4}), 132.9 (C^{F3}), 132.4 (C$^{F3'/F4'}$), 132.0 (C^{C3}), 131.8 (C^{F4}), 128.5 (C^{A5}), 128.2 (C$^{E3+E3'+E4+E4'+G3+G4}$), 127.5 (C^{C2}), 127.5 (C^{D3+D4}), 124.2 (C^{A3}), 121.7 (C^{meso-D}), 121.0 (C^{B3}), 120.9 (C^{meso-E}), 120.2 (C^{meso-G}). ESI MS m/z 1017.1 $[M]^{2+}$ (calc. 1016.7). Satisfactory elemental analysis was not obtained.

[Fe(1)$_2$][PF$_6$]$_2$. Compound **1** (56 mg, 0.057 mmol, 1 eq.) and FeCl$_2$ (7.2 mg, 0.057 mmol, 1 eq.) were dissolved in dry EtOH (20 mL) under N$_2$ and the solution was stirred at room temperature overnight. An excess of saturated aqueous NH$_4$PF$_6$

was then added. The precipitate that formed was collected by centrifuging, then was washed with H$_2$O and Et$_2$O (3 × 5 mL each). The residue was dissolved in MeCN. Solvent was removed under reduced pressure and $[Fe(1)_2][PF_6]_2$ was isolated as a dark purple powder (47 mg, 0.02 mmol, 70%). ^{1}H NMR (500 MHz, CD$_3$CN) δ/ppm: 9.22 (s, 4H, H^{B3}), 8.88-8.91 (m, 6H, H$^{F3/F4/F3'/F4'+H3}$), 8.86 (s, 4H, H^{I3+I4}), 8.82 (d, J = 4.54 Hz, 4H, H$^{F3+F4/F3'+F4'}$), 8.75 (d, J = 7.97 Hz, 4H, H^{A3}), 8.30-8.33 (m, 4H, H^{G2}), 8.23-8.27 (m, 8H, H$^{E2+E2'}$), 8.06-8.11 (m, 8H, H^{D2+C2}), 8.01 (t, J = 7.4 Hz, 4H, H^{A4}), 7.79-7.87 (m, 18H, H$^{E3+E3'+E4+E4'+G3+G4}$), 7.76 (d, J = 7.6 Hz, 4H, H^{C3}), 7.51 (t, J = 7.5 Hz, 2H, H^{D4}), 7.43 (t, J = 7.4 Hz, 4H, H^{D3}), 7.32 (d, J = 5.5 Hz, 4H, H^{A6}), 7.21 (t, J = 6.5 Hz, 4H, H^{A5}). ^{13}C NMR (126 MHz, CD$_3$CN) δ/ppm: 161.2 (C^{B2}), 159.1 (C^{A2}), 154.2 (C^{A6}), 151.5 (C^{B4}), 151.8/151.3/151.1/150.9/148.3/147.0 (C$^{F2+F5+F2'+F5'+H2+H4+H5+I2+I5}$), 143.9 (C$^{G1+E1+E1'}$), 143.4 (C^{C1}), 143.0 (C^{D1}), 139.7 (C^{A4}), 137.0 (C^{D2}), 135.7 (C^{H3}), 135.3 (C$^{G2+E2+E2'}$), 134.3 (C^{C4}), 133.4/132.8/132.2 (C$^{F3+F4+F3'+F4'}$), 132.7 (C^{I3+I4}), 132.3 (C^{C3}), 128.5 (C^{G3+G4}), 128.3 (C^{A5}), 127.9 (C^{D4}), 127.6 (C^{C2}), 127.5 (C$^{E3+E3'+E4+E4'}$), 127.1 (C^{D3}), 124.9 (C^{A3}), 122.9 (C^{meso-E}), 122.3 (C^{B3}), 121.9 (C^{meso-D}); C^{meso-G} not resolved. ESI MS m/z 984.7 $[1+H]^+$ (calc. 984.3); 1013.4 $[M]^{2+}$ (calc. $[M]^{2+}$ 1012.7). HR-ESI MS 1013.2389 $[M–2PF_6]^{2+}$ (calc. 1013.2408). Satisfactory elemental analysis was not obtained.

[Ru(1)Cl$_3$]. Compound **1** (57 mg, 0.058 mmol, 1 eq.) and RuCl$_3$·3H$_2$O (15 mg, 0.058 mmol, 1 eq.) were dissolved in dry EtOH (10 ml) and heated at reflux for 2.5 h. A precipitate formed and was separated by centrifuging. After washing with EtOH and Et$_2$O, brown $[Ru(1)Cl_3]$ was isolated (46 mg, 0.039 mmol, 67%) and was used for the next step without further characterization.

[Ru(1)$_2$][PF$_6$]$_2$. $[Ru(1)Cl_3]$ (46 mg, 0.039 mmol), **1** (38 mg, 0.039 mmol) and N-ethylmorpholine (3 drops) were suspended in dry EtOH (3 mL) in a vial. The mixture was heated in a microwave reactor at 140 °C for 20 min and then the dark red solution was poured into saturated aqueous NH$_4$PF$_6$ (50 mL). After centrifuging, the precipitate was collected and washed with water (3 × 5 mL) and Et$_2$O (3 × 5 mL). The residue was dissolved in MeCN and purified by column chromatography (SiO$_2$, MeCN/saturated aq. KNO$_3$/water 38: 1 : 1 by volume). The first orange fraction was collected, concentrated to 3 mL and poured into saturated aqueous NH$_4$PF$_6$ (25 mL) to give a precipitate which was washed with H$_2$O and EtOH (3 × 5mL). $[Ru(1)_2][PF_6]_2$ was isolated as a purple powder (9.0 mg, 0.0038 mmol, 9.7%). ^{1}H NMR (500 MHz, CD$_3$CN) δ/ppm: 9.02 (s, 4H, H^{B3}), 8.90 (m, 4H, H$^{F3+F4/F3'+F4'}$), 8.86 (s, 6H, H$^{I3+I4+H3}$), 8.76-8.83 (m, 8H, H$^{F3/F4/F3'/F4'+A3}$), 8.28-8.32 (m, 4H, H^{G2}), 8.25 (m, 8H, H$^{E2+E2'}$), 8.04 (m, 4H, H^{A4}), 8.00 (d, J = 7.3 Hz, 4H, H^{D2}), 7.93 (d, J = 7.53 Hz, 4H, H^{C2}), 7.70-7.86 (m, 18H, H$^{E3+E4+E3'+E4'+G3+G4}$), 7.67 (d, J = 7.53 Hz, 4H, H^{C3}), 7.56 (ddd, J = 5.7, 1.5, 0.6 Hz, 4H, H^{A6}), 7.46 (t, J = 7.6 Hz, 2H, H^{D4}), 7.36 (t, J = 7.5 Hz, 4H, H^{D3}), 7.22 (ddd, J = 7.2, 5.7, 1.3 Hz, 4H, H^{A5}). ^{13}C NMR (126 MHz, CD$_3$CN) δ/ppm: 159.3 (C^{A2}), 156.5 (C^{B2}), 153.5 (C^{A6}), 151.9/151.2/151.0/148.2/147.0 (C$^{F2+F5+F2'+F5'+H2+H4+H5+I2+I5}$), 149.4 (C^{B4}), 143.9 (C$^{G1+E1+E1'}$), 143.1 (C^{C1}), 142.9 (C^{D1}), 139.2 (C^{A4}), 137.0 (C^{D2}), 135.4 (C^{H3}),

135.35 (C$^{G2+E2+E2'}$), 135.3, 134.5 (C^{C4}), 133.2/132.9/132.85/132.4 (C$^{F3+F4+F3'+F4'+I3+I4}$), 132.3 (C^{C3}), 128.6 (H^{A5}), 128.0 (C^{D4}), 127.6 (C$^{E3+E3'+E4+E4'+G3+G4}$), 127.5 (C^{C2}), 127.1 (C^{D3}), 125.7 (C^{A3}), 122.9 (C^{meso-D}), 122.2 (C^{B3}), 121.9 (C^{meso-E}), 121.3 (C^{meso-G}). MALDI m/z 984.3 [ligand+H]$^+$ (calc. 984.3). HR-ESI MS 1034.2257 [M–2PF$_6$]$^{2+}$ (calc. 1034.2243). Satisfactory elemental analysis was not obtained.
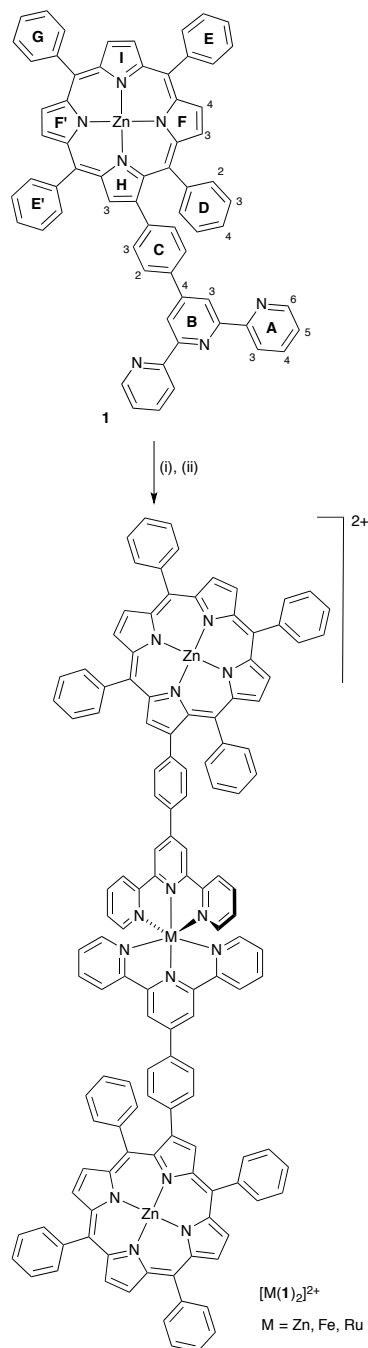
Scheme 1. Synthetic routes to [Zn(**1**)$_2$][PF$_6$]$_2$ (i) Zn(OAc)$_2$ 0.5 eq., MeOH; (ii) NH$_4$PF$_6$; [Fe(**1**)$_2$][PF$_6$]$_2$ (i) FeCl$_2$ 0.5 eq., MeOH; ii) NH$_4$PF$_6$; [Ru(**1**)$_2$][PF$_6$]$_2$ (i) RuCl$_3$·3H$_2$O, 1 eq., EtOH, reflux; ii) **1**, N-ethylmorpholine, 140 °C, 20 min under microwave conditions, followed by addition of NH$_4$PF$_6$. Atom labels are for NMR spectroscopic assignments.

Results and discussion

Synthesis and characterization of [Zn(1)$_2$][PF$_6$]$_2$, [Fe(1)$_2$][PF$_6$]$_2$ and [Ru(1)$_2$][PF$_6$]$_2$

The complexes [Zn(**1**)$_2$][PF$_6$]$_2$ and [Fe(**1**)$_2$][PF$_6$]$_2$ were prepared by the reaction of two equivalents of metalloligand **1** with zinc(II) acetate or iron(II) chloride, respectively, followed by anion exchange. A two-step approach[24] was used for the preparation of [Ru(**1**)$_2$][PF$_6$]$_2$, starting with treatment of RuCl$_3$·3H$_2$O with one equivalent of **1** to give [Ru(**1**)Cl$_3$]. This was then was reacted with a second equivalent of **1** in the presence of N-ethylmorpholine which acts as a reducing agent. Anion exchange using NH$_4$PF$_6$ led to the formation of [Ru(**1**)$_2$][PF$_6$]$_2$. The positive-mode electrospray mass spectra of [Zn(**1**)$_2$][PF$_6$]$_2$ and [Fe(**1**)$_2$][PF$_6$]$_2$ in MeCN showed peak envelopes at m/z 1017.1 and 1013.4, respectively, with half-mass peak separations confirming the double charge on the [M(**1**)$_2$]$^{2+}$ ions. For both [Fe(**1**)$_2$]$^{2+}$ and [Zn(**1**)$_2$]$^{2+}$ isotope distributions were consistent with those calculated. For [Fe(**1**)$_2$][PF$_6$]$_2$, the base peak at m/z 984.7 was assigned to [**1**+H]$^+$. Mass spectrometric characterization of [Ru(**1**)$_2$][PF$_6$]$_2$ using MALDI gave peaks at m/z 984.8 and 921.7 assigned to [**1**+H]$^+$ and [**1**–Zn+3H]$^+$ (calculated values = 983.3 and 922.4, respectively). In the high-resolution ESI MS of [Fe(**1**)$_2$][PF$_6$]$_2$ and [Ru(**1**)$_2$][PF$_6$]$_2$, peak envelopes for [Fe(**1**)$_2$]$^{2+}$ and [Ru(**1**)$_2$]$^{2+}$. Definitive evidence for the formation of the complexes was obtained from NMR spectroscopy and from the photophysical and electrochemical properties.

The NMR spectroscopic data for the three complexes were in accord with the structures shown in Scheme 1. Fig. 1 compares the ^{1}H NMR spectra of **1** (CDCl$_3$) and [Fe(**1**)$_2$][PF$_6$]$_2$ (CD$_3$CN); differences in solubilities did not allow a common solvent to be used. ^{1}H and ^{13}C NMR spectra were fully assigned using COSY, NOESY, HMQC and HMBC spectra. The shift to lower frequency for the resonance for H^{A6} is typical upon formation of an {M(tpy)$_2$} unit, being a consequence of H^{A6} lying over the π-cloud of the adjacent, orthogonal ligand. The movement of this signal is less pronounced on going from **1** to [Zn(**1**)$_2$][PF$_6$]$_2$ than from **1** to [Fe(**1**)$_2$][PF$_6$]$_2$ or [Ru(**1**)$_2$][PF$_6$]$_2$. A second diagnostic signal is that for ^{13}C nucleus C^{B4} (see Scheme 1) which is assigned on the basis of an HMBC cross peak to proton H^{C2}. Significantly, the trends observed for signals H^{A6} and C^{B4} as the metal ion in the {M(tpy)$_2$} unit changes from Fe to Ru to Zn are also seen in other series of [M(tpy)$_2$]$^{2+}$ complexes as demonstrated in Table 1 for the complexes containing 4'-(4-tolyl-2,2':6',2"-terpyridine) (ttpy). In the case of zinc(II), the NMR spectroscopic data are consistent with the formation of [Zn(**1**)$_2$][PF$_6$]$_2$ rather than a 5-coordinate complex of type [Zn(**1**)(OAc)$_2$].[25,26,27,28]

Table 1. Trends in the chemical shifts for H[A6], H[B3] and C[B4] in [M(**1**)$_2$][PF$_6$]$_2$ and the reference complexes [M(ttol)$_2$][PF$_6$]$_2$ (CD$_3$CN).

Complex	H[A6] δ / ppm	C[B4] δ / ppm	Ref.
[Fe(**1**)$_2$][PF$_6$]$_2$	7.32	151.4	This work
[Fe(ttol)$_2$][PF$_6$]$_2$	7.18	151.6	29
[Ru(**1**)$_2$][PF$_6$]$_2$	7.56	149.4	This work
[Ru(ttol)$_2$][PF$_6$]$_2$	7.43	149.3	29,30
[Zn(**1**)$_2$][PF$_6$]$_2$	8.31	156.6	This work
[Zn(ttol)$_2$][PF$_6$]$_2$	7.82	157.3	31, This work[a]

[a]See ESI.
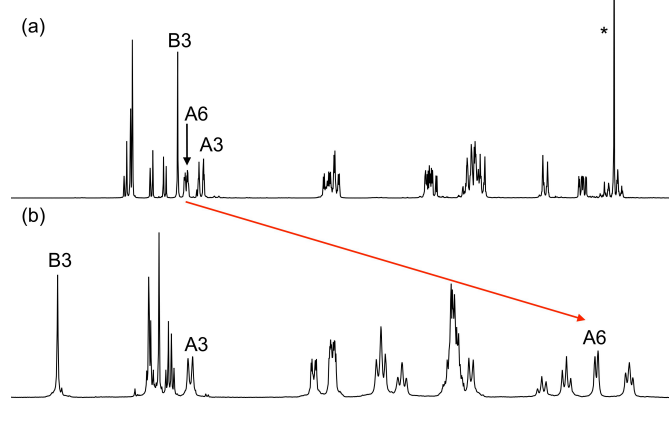
Fig. 1. 500 MHz ^{1}H NMR spectra of (a) **1** in CDCl$_3$, and (b) [Fe(**1**)$_2$][PF$_6$]$_2$ in CD$_3$CN. In (a), * = residual CHCl$_3$. Chemical shifts are in δ / ppm

Cyclic voltammetry

The electrochemical data for [Zn(**1**)$_2$][PF$_6$]$_2$, [Fe(**1**)$_2$][PF$_6$]$_2$ and [Ru(**1**)$_2$][PF$_6$]$_2$ are given in Table 2 and cyclic voltammograms (CVs) are shown in Fig. S1–S3†. The data are compared with those of **1** and the heteroleptic complex [Ru(**1**)(**2**)][PF$_6$]$_2$ where **2** is diethyl (4-([2,2':6',2"-terpyridin]-4'-yl)phenyl)phosphonate.[8] The CV for [Zn(**1**)$_2$][PF$_6$]$_2$ exhibits two porphyrin-based oxidations, the potentials for which agree well with those of **1**. An additional reversible, metal-centred oxidation is observed for each of [Fe(**1**)$_2$][PF$_6$]$_2$ and [Ru(**1**)$_2$][PF$_6$]$_2$; for the latter, this appears at +0.89 V, consistent with that reported for [Ru(**1**)(**2**)][PF$_6$]$_2$.[8] However, for [Fe(**1**)$_2$][PF$_6$]$_2$, the Fe$^{2+/3+}$ process overlaps with the [Zn(TPP)]$^+$/[Zn(TPP)]$^{2+}$ couple. Differential pulse voltammetry was performed to confirm that the first and second oxidations corresponded, respectively, to two- and three-electron processes, specifically, one-electron oxidations of two [Zn(TPP)] units at +0.37 and +0.65 V, and the Fe^{2+}/Fe^{3+} process at +0.65 V. This value is at lower potential than that in [Fe(tpy)$_2$][PF$_6$]$_2$ (+0.77 V)[32] consistent with the introduction of the electron-releasing substituents[24] in the 4'-position of the tpy domain of **1**.

Table 2. Electrochemical data for [Zn(**1**)$_2$][PF$_6$]$_2$, [Fe(**1**)$_2$][PF$_6$]$_2$ and [Ru(**1**)$_2$][PF$_6$]$_2$ in MeCN solution compared to **1** and the heteroleptic complex [Ru(**1**)(**2**)][PF$_6$]$_2$ in MeCN measured using cyclic voltammetry. Potentials are referenced to Fc/Fc$^+$ with 0.1 M [^{n}Bu$_4$N][PF$_6$] as supporting electrolyte and a scan rate of 0.1 V s^{-1} (ir = irreversible).[a]

Compound	$E_{1/2}^{ox}$/Va	$E_{1/2}^{red}$/V	$E_{1/2}^{ox}$–$E_{1/2}^{red}$ / V	Reference
1	+0.34 (57) +0.66 (84)	−1.76[ir] −1.97[ir] −2.09[ir] −2.27[ir]	2.10	8
[Zn(**1**)$_2$][PF$_6$]$_2$	+0.38 (56) +0.67 (92)	−1.26[ir] −1.89[ir]	1.64	This ref.
[Fe(**1**)$_2$][PF$_6$]$_2$	+0.37 (83) +0.65 (92)	−1.35[ir] −1.92[ir] −2.43[ir]	1.72	This ref.
[Ru(**1**)$_2$][PF$_6$]$_2$	+0.39 (74) +0.67 (65) +0.89 (65)	−1.30[ir] −1.92[ir]	1.69	This ref.
[Ru(**1**)(**2**)][PF$_6$]$_2$	+0.39 (56) +0.67 (56) +0.88 (65)	−1.56[ir] −1.87[ir] −2.21[ir]	1.95	8

[a] Values in parentheses = E$_{pe}$ – E$_{pa}$ in mV. A glassy carbon electrode was replaced the platinum one (see Experimental section).

Table 3. Absorption spectra of **1**,[8] [Zn(**1**)$_2$][PF$_6$]$_2$ (4 × 10^{-7} mol dm^{-3}), [Fe(**1**)$_2$][PF$_6$]$_2$ (1 × 10^{-6} mol dm^{-3}) and [Ru(**1**)$_2$][PF$_6$]$_2$ (7 × 10^{-7} mol dm^{-3}) in MeCN solution.

Compound	λ_{max} / nm (ε_{max} / dm^3 mol^{-1} cm^{-1})				
	tpy-centred	Soret	Q1	Q2	MLCT
1	285 (56,000), 315 (41000)	427 (520,000)	560 (26,000)	599 (9,500)	
[Zn(**1**)$_2$][PF$_6$]$_2$	285 (100,000), 327 (99,000), 337 (96,000)	426 (660,000)	560 (41,000)	600 (17,000)	
[Fe(**1**)$_2$][PF$_6$]$_2$	284 (105,000), 321 (115,000)	426 (840,000)	568[a] (88,000)	597[a] (35,000)	~573[a] (88,000)
[Ru(**1**)$_2$][PF$_6$]$_2$	283 (82,000), 310 (102,000)	425 (670,000)	559 (47,000)	599 (16,000)	495 (62,000)

[a]Q1 and MLCT, and Q2 and MLCT bands overlap. See the discussion of the spectroelectrochemistry.

Absorption spectra

Fig. 2 compares the solution absorption spectra of [Zn(**1**)$_2$][PF$_6$]$_2$, [Fe(**1**)$_2$][PF$_6$]$_2$ and [Ru(**1**)$_2$][PF$_6$]$_2$, and the data are presented in Table 3. The assignment of the transitions follows the typical nomenclature for porphyrin spectroscopy, and the observed Soret and Q bands are typical for a metallated porphyrin.[33] The strong absorption centered at 426 nm corresponds to the Soret band (S$_0$ ← S$_2$ transition), while the Q bands appear as two weaker absorptions to lower energy. Their separation reflects that of the vibrational levels (0,0) and (0,1) from the S$_0$ ← S$_1$ transition. The bands in the UV region arise

from tpy-centered (ligand centred, LC) $\pi^* \leftarrow \pi$ transitions. The absorption spectrum of $[Zn(\mathbf{1})_2][PF_6]_2$ exhibits only these tpy-centred bands as expected for a complex containing a d^{10} metal ion, whereas a metal-to-ligand charge-transfer (MLCT) band is also present in the spectra of $[Fe(\mathbf{1})_2][PF_6]_2$ and $[Ru(\mathbf{1})_2][PF_6]_2$. In the latter, the MLCT band is clearly visible at 495 nm, but for $[Fe(\mathbf{1})_2][PF_6]_2$, it overlaps with the Q bands (Table 3). The assignments were verified by the results of the spectroelectrochemical investigations described below.
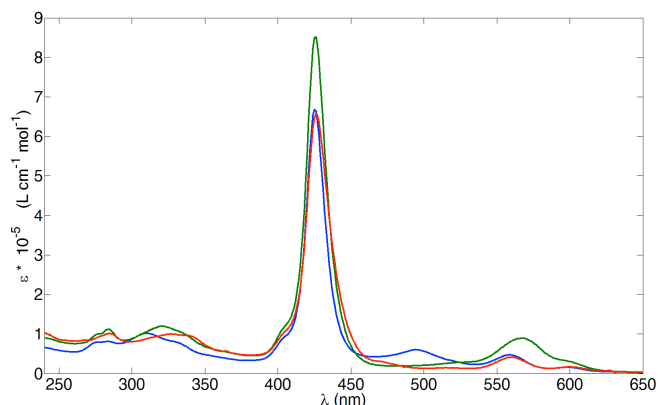
Fig. 2 Absorption spectra of MeCN solutions of $[Zn(\mathbf{1})_2][PF_6]_2$ (red, MeCN), $[Fe(\mathbf{1})_2][PF_6]_2$ (green) and $[Ru(\mathbf{1})_2][PF_6]_2$ (blue). See Table 3 for concentrations and values of λ_{max} and ε_{max}.

Spectroelectrochemistry: anodic region

The spectroelectrochemistry of the complex [Zn(TPP)] has been reported.[34] Initial oxidation leads to a π-radical cation, the Soret band of which is about half the intensity of the original Soret band. At the same time, the Q bands disappear and an absorption with $\lambda_{max} \approx 650$ nm grows in. Although $[Zn(TPP)]^+$ is stable on the experimental timescale, the second oxidation to $[Zn(TPP)]^{2+}$ is irreversible and the dication is transformed by further chemical reactions. For the homoleptic complexes $[M(\mathbf{1})_2][PF_6]_2$ with M = Zn, Fe or Ru, it was possible to oxidize the porphyrin moiety either reversibly or irreversibly, depending on the potential applied during the experiment. For potentials ≤ 1.3 V, the redox processes are almost completely reversible, while for peak-potentials >1.6 V it was not possible to return the complex to its initial state. We start by discussing the spectroelectrochemistry for both the irreversible and the reversible cases.

Fig. S4a† shows the absorption spectra of $[Zn(\mathbf{1})_2][PF_6]_2$ recorded before and after an oxidative cycle up to +2.0 V. The Soret band decreases in intensity and red-shifts as the potential is increased to more positive values. Fig. S4b† shows the set of 41 scans covering the oxidative cycle and the irreversibile oxidation is consistent with that reported for [Zn(TPP)].[34] The Q bands disappear during the oxidation, and a new band develops at 667 nm (Fig. S4†). The tpy-based absorption band is unchanged during the oxidation cycle. Fig. S5† shows the results of the spectroelectrochemistry if the scan is interrupted at +1.3 V and then reversed. The recovery of the absorption bands is almost complete and a partial decrease in the intensity

of the Soret band is the only significant difference with respect to the initial spectrum.

Fig. 3 shows spectroelectrochemical data for the oxidative cycle of $[Fe(\mathbf{1})_2][PF_6]_2$ upon scanning from 0 to +2.0 V and back. The spectroscopic behavior of the [Zn(TPP)] moiety is comparable to that of $[Zn(\mathbf{1})_2][PF_6]_2$ discussed above. Upon oxidation, the Q bands are the first to disappear, followed by the MLCT band at 573 nm. The exact position for the MLCT maximum can only be found by analyzing one of the spectra in which the MLCT band is free of the Q band contributions. Reversing the potential, the reappearance of the MLCT band at 573 nm confirms the regeneration of the $\{Fe(tpy)_2\}^{2+}$ core. This is followed by the appearance of a new band at 666 nm. Both absorptions are present at the end of the experiment, indicating the generation of new stable chemical species. As for $[Zn(\mathbf{1})_2][PF_6]_2$, if the scan is interrupted at +1.3 V and then reversed, the redox processes involving the [Zn(TPP)] domain is reversible (Fig. S6†).

(a)

(b)

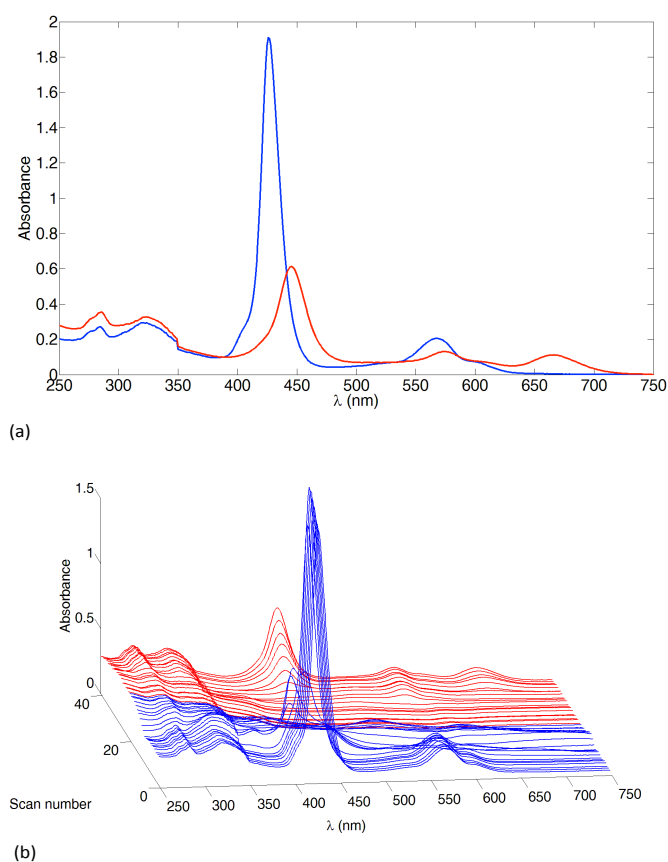**Fig. 3**. Spectroelectrochemical data for the oxidative cycle of $[Fe(\mathbf{1})_2][PF_6]_2$ (≈ 0.6 mM in MeCN, $[^nBu_4N][PF_6]$ supporting electrolyte). (a) Absorption spectra before (blue line) and after (red line) the oxidative cycle. (b) A spectrum was recorded every 0.1 V, starting from 0 V (first blue line at the front) to +2 V (last blue line) and back from +2 V (first red line) to 0 V (last red line). The potential is referenced with respect to the Fc/Fc$^+$ redox couple with the same cell under the same experimental conditions.

The irreversible spectroelectrochemical oxidative cycle for $[Ru(\mathbf{1})_2][PF_6]_2$ is presented in Fig. S7†. Reducing the potential window and reversing the scan at +1.3 V results in the changes

presented in Fig. 4. The spectroscopic changes associated with the first oxidation involve the porphyrin, with the loss of Q bands, and a blue-shift (to 410 nm) and loss in intensity of the Soret band; the MLCT band at 495 nm is unchanged. In the second oxidation step both the Soret and the MLCT band are lost. Reversing the scan regenerates the MLCT band, with the Soret band appearing in its blue-shifted form. Bringing the potential back to the initial 0 V, recovers the original Soret and Q bands, with intensities that compare well with those of the original spectrum (Fig. 4a).

(a)

(b)
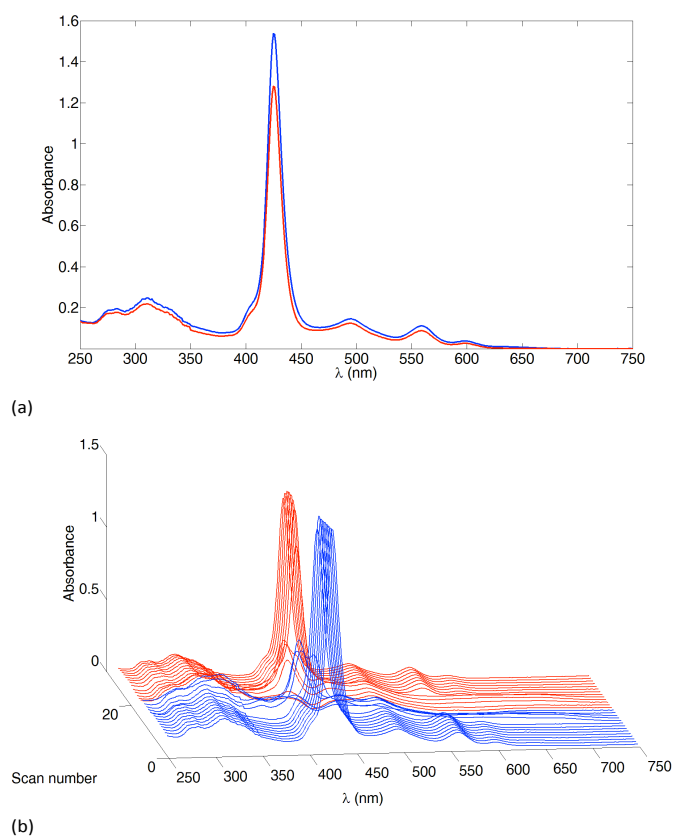
Fig. 4. Spectroelectrochemical data for the oxidative cycle of $[Ru(\mathbf{1})_2][PF_6]_2$ (≈ 0.5 mM in MeCN, $[^nBu_4N][PF_6]$ supporting electrolyte). (a) Absorption spectra before (blue line) and after (red line) the oxidative cycle. (b) A spectrum was recorded every 0.1 V, starting from 0 V (first blue line at the front) to +1.3 V (last blue line) and back from +1.3 V (first red line) to 0 V (last red line). See caption to Fig. 3 for referencing to Fc/Fc$^+$.

Spectroelectrochemistry: cathodic region

In this section, we focus on the reduction processes, for which only irreversible processes were observed in the CVs (Table 2). [Zn(TPP)] can be reduced to mono- and dianionic forms, the latter of which is only stable under rigorous experimental conditions. $[Zn(TPP)]^{2-}$ has been obtained by reduction of [Zn(TPP)] with sodium, and its absorption spectrum has been recorded in THF (Soret band at 437 nm and Q bands at ~550 and ~600 nm).[35] Spectroscopic changes associated with the reduction of [Zn(TPP)] include a red-shift and a decrease in intensity of the Soret band, loss of the Q-bands in favour of a new band at ~800 nm (monoanion). Further reduction to the dianion leads to a new set of Q-bands and the disappearance of

the absorption at 800 nm.[34] Fig. S8† shows the spectroelectrochemical measurement for $[Zn(\mathbf{1})_2][PF_6]_2$ during a reductive cycle from 0 to −2 V and back. The main electronic structural changes occur at the porphyrin unit and are consistent with the spectroscopic changes detailed above, with each [Zn(TPP)] domain in $[Zn(\mathbf{1})_2][PF_6]_2$ undergoing two reductions (Fig. 5). The doubly-reduced species is characterized by two broad bands centered at 562 and 613 nm (green spectrum in Fig. 5). A similar situation is observed for $[Fe(\mathbf{1})_2][PF_6]_2$ in a reductive cycle from 0 to −1.8 V (scans 1 to 19 in Fig. S9†). Although the absorptions at 562 and 613 nm are at similar wavelengths and have similar relative intensities to those observed for a chlorin,[36] the lack of a Soret band (Fig. 5) rules out the latter as a possible product of the reductive process. The spectral response upon reversing the potential from −2 to 0 V is different for $[Zn(\mathbf{1})_2][PF_6]_2$ and $[Fe(\mathbf{1})_2][PF_6]_2$. In the case of $[Fe(\mathbf{1})_2][PF_6]_2$, Fig. S9† shows that all absorptions are essentially lost confirming that the reduction is chemically irreversible. For $[Zn(\mathbf{1})_2][PF_6]_2$, the Q bands at 560 and 613 nm which are present at the limit of the reductive cycle disappear during the sweep from −1.8 to −2 V, whilst the absorption in the UV region undergoes a series of changes but remains a dominant component in the spectrum (Fig. S8†).
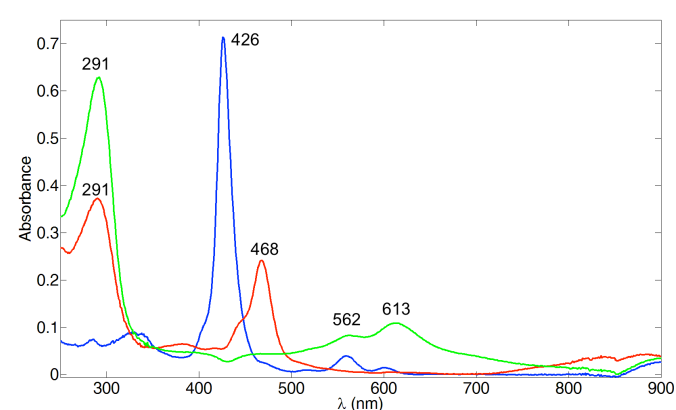

Fig. 5. Absorption spectra of neutral $[Zn(\mathbf{1})_2][PF_6]_2$ (blue), its monoanion (red corresponding to scan number 18 (-1.7 V) in Fig. S8) and its dianion (green corresponding to scan number 21 (-2 V) in Fig. S8) in MeCN.

The reductive processes for $[Zn(\mathbf{1})_2][PF_6]_2$ and $[Fe(\mathbf{1})_2][PF_6]_2$ are reversible if the potential cycle is reversed at −1.6 V (Figs. 6 and 7). The [Zn(TPP)] domains are reduced to their monoanionic forms and re-oxidized in a reversible manner. The original spectrum is recovered (albeit at a lower intensity, Fig. 6a) for $[Zn(\mathbf{1})_2][PF_6]_2$ at the end of the cycle. In contrast, for $[Fe(\mathbf{1})_2][PF_6]_2$, the porphyrin-based absorption bands are red-shifted (the Soret band shifts from 426 to 437 nm) and the shoulder of the Soret band at 405 nm becomes more distinct (Fig. 7a) after the reduction cycle. The tpy-centred absorptions and the MLCT band at ~573 nm of $[Fe(\mathbf{1})_2][PF_6]_2$ are not regenerated after the reductive cycle. The MLCT band is completely lost at the end of the experiment, leaving only Q bands at 577 and 617 nm indicating that the ligand is irreversibly chemically modified.
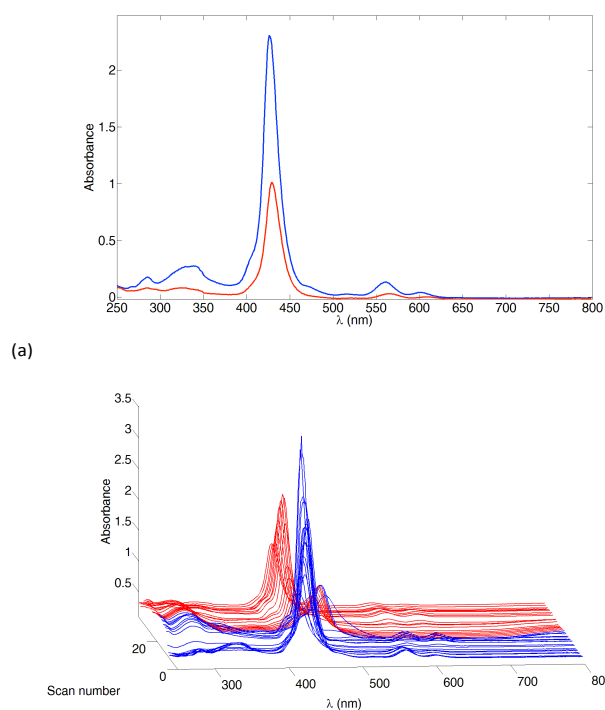
(a)

(b)

Fig. 6. Spectroelectrochemical data for the reductive cycle of [Zn(**1**)$_2$][PF$_6$]$_2$ ($\approx$ 1 mM in MeCN, [^{n}Bu$_4$N][PF$_6$] supporting electrolyte). (a) Absorption spectra before (blue line) and after (red line) the reductive cycle (0 to −1.6 to 0 V). (b) A spectrum was recorded every 0.1 V, starting from 0 V (first blue line at the front) to −1.6 V (last blue line) and back from −1.6 V (first red line) to 0 V (last red line). See caption to Fig. 3 for referencing to Fc/Fc$^+$.

Fig. S10† shows the spectroelectrochemical response of [Ru(**1**)$_2$][PF$_6$]$_2$ during the reductive cycle when the potential is taken to −2 V. The irreversible changes are reminiscent of those for [Zn(**1**)$_2$][PF$_6$]$_2$, with an additional loss of the MLCT band at 495 nm. Fig. 8 displays the redox behavior of [Ru(**1**)$_2$][PF$_6$]$_2$ in the cathodic region if the reduction cycle is reversed at −1.6 V. Between 0 and −0.6 V, the Soret band loses intensity and shifts towards the red (434 nm). In addition, there is a complete loss of tpy-based absorptions, as well as the MLCT and Q bands. Reduction between −0.6 and −1.3 V results in an enhancement of the Soret band (437 nm) and recovery of the Q bands. After reversing the scan, the Soret band again diminishes but is regenerated at ∼ −0.6 V. The MLCT band is regenerated just before the scan is completed (Fig. 8b). A comparison of Fig. 7a and 8a reveals a similar relationship between the starting complex ([Fe(**1**)$_2$][PF$_6$]$_2$ or [Ru(**1**)$_2$][PF$_6$]$_2$) and the final product of the reductive cycle, with the exception of the different positions of the MLCT bands associated with the {Fe(tpy)$_2$}$^{2+}$ and {Ru(tpy)$_2$}$^{2+}$ domains.

(a)

(b)

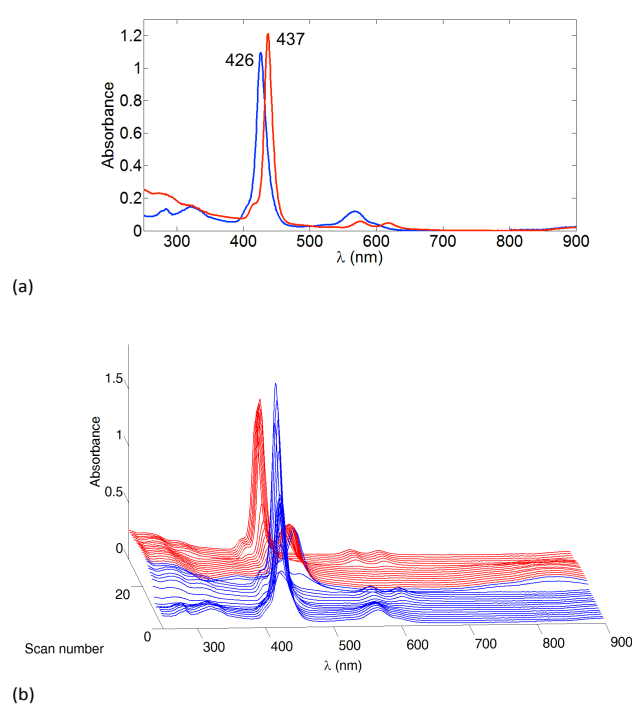**Fig. 7**. Spectroelectrochemical data for the reductive cycle of [Fe(**1**)$_2$][PF$_6$]$_2$ ($\approx$ 1 mM in MeCN, [^{n}Bu$_4$N][PF$_6$] supporting electrolyte). (a) Absorption spectra before (blue line) and after (red line) the reductive cycle. (b) A spectrum was recorded every 0.1 V, starting from 0 V (first blue line at the front) to −1.6 V (last blue line) and back from −1.6 V (first red line) to 0 V (last red line). See caption to Fig. 3 for referencing to Fc/Fc$^+$.
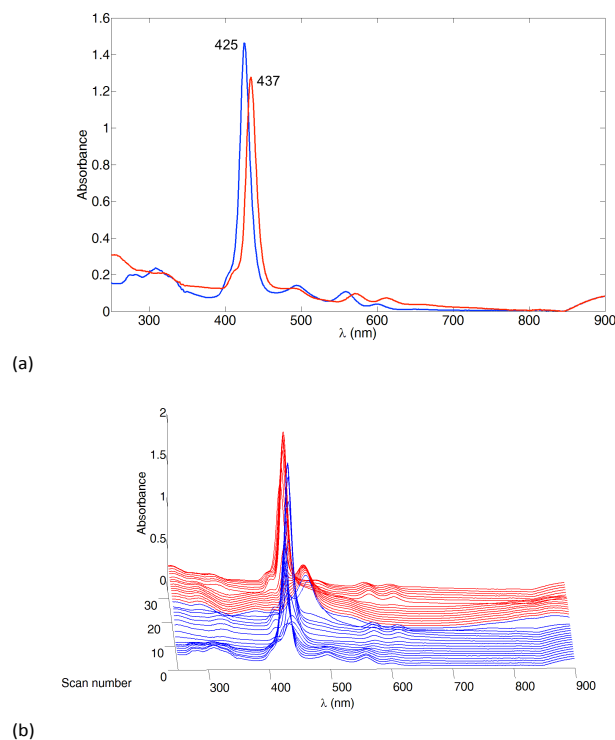

(a)

(b)

Fig. 8. Spectroelectrochemical data for the reductive cycle of [Ru(**1**)$_2$][PF$_6$]$_2$ ($\approx$ 1 mM in MeCN, [^{n}Bu$_4$N][PF$_6$] supporting electrolyte). (a) Absorption spectra before (blue line) and after (red line) the oxidative cycle. (b) A spectrum was recorded every 0.1 V, starting from 0 V (first blue line at the front) to −1.6 V (last blue line)

and back from −1.6 V (first red line) to 0 V (last red line). See caption to Fig. 3 for referencing to Fc/Fc$^+$.

Transient absorption spectra

Acetonitrile solutions of [Zn($\mathbf{1}$)$_2$][PF$_6$]$_2$ and [Fe($\mathbf{1}$)$_2$][PF$_6$]$_2$ were excited at 550 nm (corresponding to the Q(1,0) transition), while [Ru($\mathbf{1}$)$_2$][PF$_6$]$_2$ was excited at 532 nm. The transient absorption spectrum of [Zn($\mathbf{1}$)$_2$][PF$_6$]$_2$ is presented in Fig. 9. This correlates well with the triplet-triplet spectrum of [Zn(TPP)].[37,38] A broad absorption is present at low energy, extending from 600 to 800 nm, in agreement with the literature spectrum.[38] Another fingerprint of the T$_1$ state is a weak forbidden transition in the near infra-red (832 nm). It was not possible to record such a signal in the transient absorption spectra of either [Zn($\mathbf{1}$)$_2$][PF$_6$]$_2$ or [Fe($\mathbf{1}$)$_2$][PF$_6$]$_2$, but it is visible in the spectrum of a deaerated solution of [Ru($\mathbf{1}$)$_2$][PF$_6$]$_2$ (Fig. 10). The transient absorption spectrum for [Fe($\mathbf{1}$)$_2$][PF$_6$]$_2$ (Fig. S11†) was similar to that of [Zn($\mathbf{1}$)$_2$][PF$_6$]$_2$. Excitation was performed at 550 nm, where both Fe(II)-MLCT and Q(0,1) bands absorb. The iron(II) ^{3}MLCT state is known to rapidly deactivate through ^{3}MC d-states.[39,40] Hence, it is reasonable to assume that the resulting triplet-triplet spectrum is solely due to absorption by the Q-band.
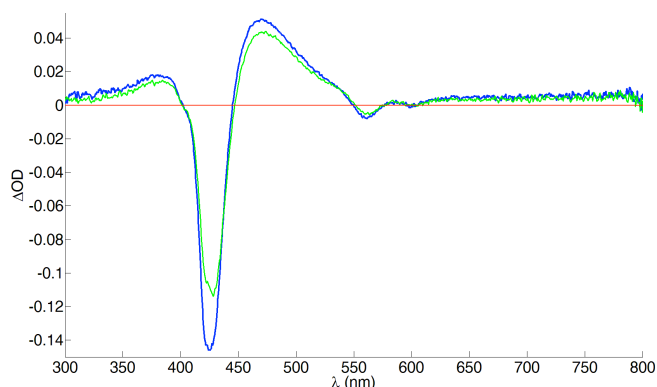

Fig. 9. Transient absorption spectrum of [Zn($\mathbf{1}$)$_2$][PF$_6$]$_2$ (MeCN, ≈ 2 x 10^{-6} M, room temperature), λ_{ex} = 550 nm. Acquisition time 200ns, 5 acquisitions. Blue line deaerated solution, green line air-equilibrated solution.
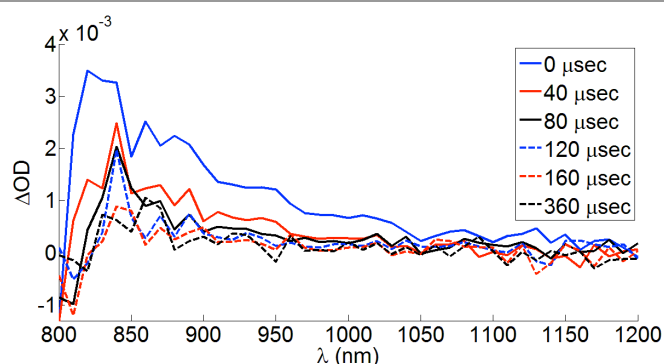

Fig. 10. NIR transient absorption spectrum of [Ru($\mathbf{1}$)$_2$][PF$_6$]$_2$ (MeCN, ≈ 2 x 10^{-6} M, room temperature), λ_{ex} = 532 nm. The spectra were reconstructed from decay curves recorded every 10 nm.

The transient absorption spectrum of an MeCN solution of [Ru($\mathbf{1}$)$_2$][PF$_6$]$_2$ is shown in Fig. S12†. Excitation at 532 nm resulted in an excited state species arising from absorption in the MLCT band of the complex. As for the other complexes, the triplet-triplet spectrum of a [Zn(TPP)] species results. In the case of [Ru($\mathbf{1}$)$_2$][PF$_6$]$_2$, the final T$_1$ state is populated through triplet-to-triplet energy transfer from the Ru(II)-^{3}MLCT state. A rate constant for the transfer could not be determined, since it was faster than the instrumental time-resolution. A comparison can, however, be made with the transient absorption spectrum of [Ru($\mathbf{1}$)($\mathbf{2}$)][PF$_6$]$_2$; this complex also contains a [Zn(TPP)] moiety conjugated to a {Ru(tpy)$_2$}$^{2+}$ unit.[8] For [Ru($\mathbf{1}$)($\mathbf{2}$)][PF$_6$]$_2$, the energy transfer is faster than the resolution of a picosecond setup, i.e. <50 ps.[8] This precludes more detailed mechanistic investigations.

Fig. 11 shows the relative energies for the different chromophores in the series of compounds under examination. The [Zn(TPP)] S$_1$ level of 590 nm (2.1 eV) was calculated from the spectra of [Zn($\mathbf{1}$)$_2$][PF$_6$]$_2$, and from the crossing point between the Q(0,0) bands in absorption and emission. We have previously reported the [Zn(TPP)] S$_2$ level.[8] The ^{1}MLCT energy level was derived from the absorption maximum of [Fe($\mathbf{1}$)$_2$][PF$_6$]$_2$ or [Ru($\mathbf{1}$)$_2$][PF$_6$]$_2$, and the ^{3}MLCT level from the emission maximum of the analogous [Ru(pytpy)$_2$][PF$_6$]$_2$ (pytpy = 4'-(4-pyridyl)-2,2':6',2"-terpyridine) in MeCN (655 nm,[41] 1.89 eV) since the ^{3}MLCT state of [Ru($\mathbf{1}$)$_2$][PF$_6$]$_2$ is not emissive at room temperature in solution. Contrary to other [Ru(4'-Xtpy)$_2$]$^{2+}$ complexes, the emission of which are weak but detectable,[42] [Ru($\mathbf{1}$)$_2$][PF$_6$]$_2$ exhibits emission behaviour centred on the porphyrin moiety even upon direct MLCT excitation. Finally, the [Zn(TPP)] T$_1$ energy (770 nm, 1.61 eV) was obtained from literature data.[43] The relative energies of the states allow us to draw the energy transfer scheme presented in Scheme 2. For [Zn($\mathbf{1}$)$_2$][PF$_6$]$_2$, upon excitation to S$_1$, efficient intersystem crossing to T$_1$ occurs. For [Fe($\mathbf{1}$)$_2$][PF$_6$]$_2$, excitation of the ^{1}MLCT transition is followed by fast deactivation into the ^{3}MC state,[39,40] which then thermally decays to the ground state. For [Ru($\mathbf{1}$)$_2$][PF$_6$]$_2$, excitation of the ^{1}MLCT transition is followed by fast intersystem crossing to ^{3}MLCT. Triplet-to-triplet energy transfer takes place, leading to the [Zn(TPP)] T$_1$ state, which then regenerates the ground state by non-radiative decay.
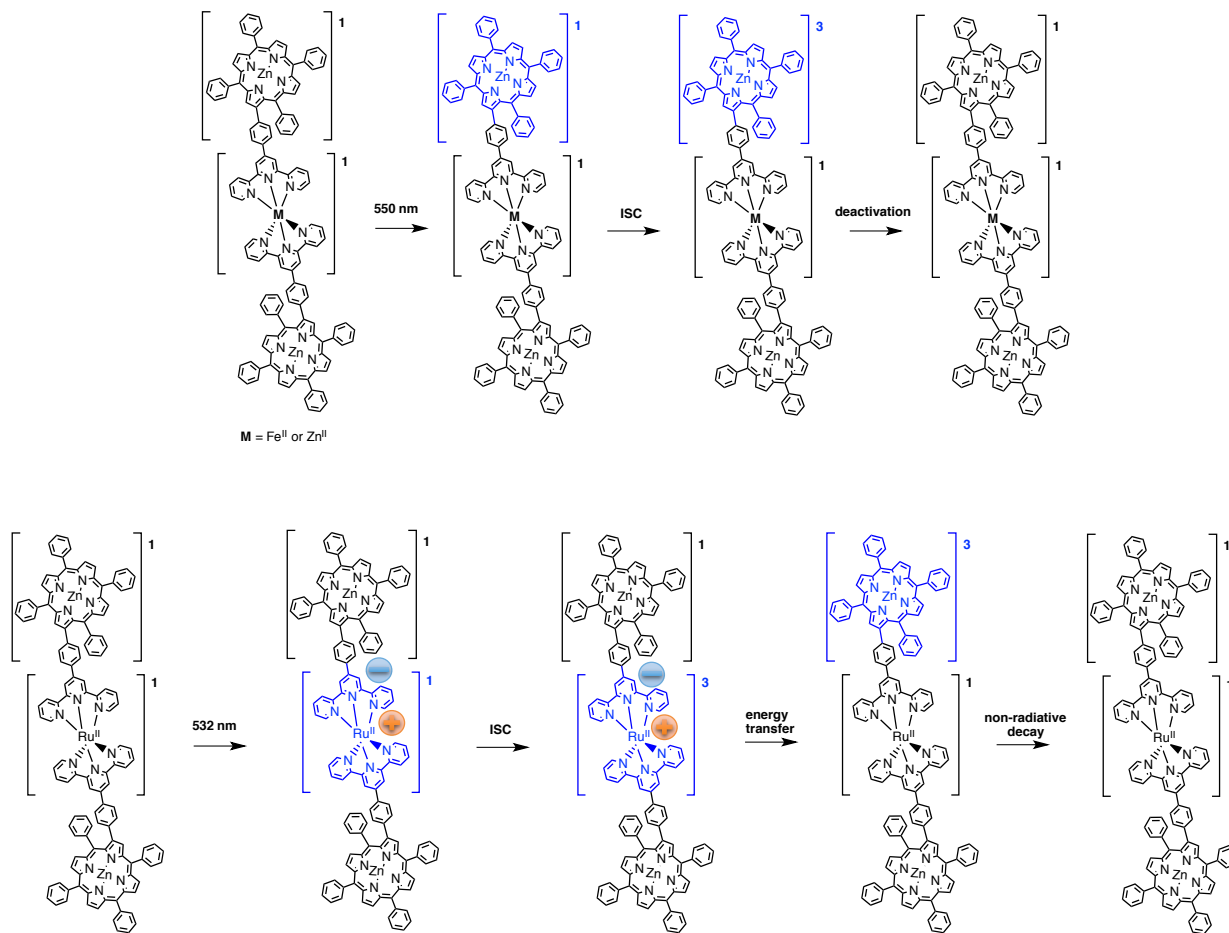
Scheme 2. Energy-transfer scheme upon Q-band excitation in $[Zn(\mathbf{1})_2][PF_6]_2$ and $[Fe(\mathbf{1})_2][PF_6]_2$ (top) or MLCT excitation in $[Ru(\mathbf{1})_2][PF_6]_2$ (bottom). ISC = intersystem crossing. The blue colour refers to the localised excited state.
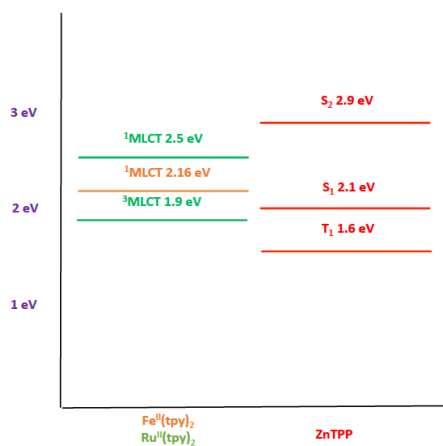

Fig. 11. Energy level diagram for the chromophores in the complexes reported in this paper. [Zn(TPP)] levels (red and black) are common to all complexes. $[Ru(\mathbf{1})_2][PF_6]_2$ MLCT levels are shown in green, whilst that for $[Fe(\mathbf{1})_2][PF_6]_2$ is shown in orange.

Conclusions

The syntheses of the homoleptic complexes $[Zn(\mathbf{1})_2][PF_6]_2$, $[Fe(\mathbf{1})_2][PF_6]_2$ and $[Ru(\mathbf{1})_2][PF_6]_2$ in which ligand $\mathbf{1}$ is a porphyrinatozinc(II)-decorated tpy have been described. ^{1}H and ^{13}C NMR spectroscopies and mass spectrometry were used to characterize the complexes. Cyclic voltammetry shows that in solution, each complex undergoes two, reversible porphyrin-centred oxidation processes, and each of $[Fe(\mathbf{1})_2][PF_6]_2$ and $[Ru(\mathbf{1})_2][PF_6]_2$ also exhibits a reversible metal-centred oxidation for at +0.65 and +0.89 V, respectively (vs. Fc/Fc$^+$). In the CV, the Fe^{2+}/Fe^{3+} process coincides with one porphyrin-centred process but was unambiguously established by using DPV. Apart from the additional MLCT bands at 573 and 495 nm, respectively, for $[Fe(\mathbf{1})_2][PF_6]_2$ and $[Ru(\mathbf{1})_2][PF_6]_2$, the absorption spectra of the homolpetic complexes are similar to the spectrum of metalloligand $\mathbf{1}$. A detailed spectroelectrochemical investigation establishes the conditions under which oxidative processes are reversible; with peak-potentials ≤ 1.3 V, the redox processes are almost completely reversible, while scanning beyond +1.6 V irreversibly oxidizes the [Zn(TPP)] units. $[Zn(\mathbf{1})_2][PF_6]_2$, $[Fe(\mathbf{1})_2][PF_6]_2$ and $[Ru(\mathbf{1})_2][PF_6]_2$ have been investigated using transient

absorption spectroscopy. For $[Zn(1)_2][PF_6]_2$, S_1 excitation leads to efficient intersystem-crossing to the T_1 state, whilst for $[Fe(1)_2][PF_6]_2$, excitation of the ^{1}MLCT transition is followed by fast deactivation to the ^{3}MC state followed by thermal decay to the ground state. Excitation of the ^{1}MLCT transition of $[Ru(1)_2][PF_6]_2$ results in an intersystem crossing to ^{3}MLCT; triplet-to-triplet energy transfer occurs giving the [Zn(TPP)] T_1 state which regenerates the ground state of the complex

Acknowledgements

Notes and references

[a]Department of Chemistry, University of Basel, Spitalstrasse 51, CH-4056 Basel, Switzerland; email: catherine.housecroft@unibas.ch
[b]Department of Chemistry, University of Basel, St. Johanns-Ring 19, CH-4056 Basel, Switzerland
†Electronic Supplementary Information (ESI) available: ^{13}C NMR spectroscopic data for $[Zn(ttpy)_2][PF_6]_2$. Fig. S1–S3: CVs of the complexes. Fig. S4–S10: Spectroelectrochemical spectra. Fig. S11-S12: Transient absorption spectra. See DOI: 10.1039/b000000x/

1   A. Harriman, F. Odobel and J.-P. Sauvage, *J. Am. Chem. Soc.*, 1995, **117**, 9461.

2   I.M. Dixon and J.-P. Collin, *J. Porphyrins Phthalocyanins*, 2001, **5**, 600.

3   A.C. Benniston, A. Harriman, C. Pariani and C.A. Sams, *Phys. Chem. Chem. Phys.*, 2006, **8**, 2051.

4   A.C. Benniston, *Phys. Chem. Chem. Phys.*, 2007, **9**, 5739.

5   A.C. Benniston, A. Harriman and P. Li, *J. Am. Chem. Soc.*, 2010, **132**, 26.

6   A. Quaranta, G. Charalambidis, C. Herrero, S. Margiola, W. Leibl, A. Coutsolelos and A. Aukauloo, *Phys. Chem. Chem. Phys.*, 2015, **17**, 24166.

7   L. Flamigni, *Chem. Rec.*, 2016, **16**, 1067.

8   A. Lanzilotto, L. A. Büldt, H. C. Schmidt, A. Prescimone, O. S. Wenger, E. C. Constable and C. E. Housecroft, *RSC Adv.*, 2016, **6**, 15370.

9   X. Liu, J. Liu, K. Jin, X. Yang, Q. Peng and L. Sun, *Tetrahedron*, 2005, **61**, 5655.

10 J.L. Allwood, A.K. Burrell, D.L. Officer, S.M. Scott, K.Y. Wild and K.C. Gordon, *Chem. Commun.*, 2000, 747.

11 D. LeGourriérec, M. Andersson, J. Davidsson, E. Mukhtar, L. Sun and L. Hammarström, *J. Phys. Chem. A*, 1999, **103**, 557.

12 I. Hamachi, S. Tsukiji, S. Shinkai and S. Oishi, *J. Am. Chem. Soc.*, 1999, **121**, 5500.

13 A. Harriman, M. Hissler, O. Trompette and R. Ziessel, *J. Am. Chem. Soc.*, 1999, **121**, 2516.

14 K. Araki, P. Losco, F.M. Engelmann, H. Winnischofer and H.E. Tona, *J. Photochem. Photobiol. A,* 2001, **142**, 25.

15 J.M. Lintuluoto, V.V. Borovkov, G.A. Hembury and Y. Inoue, *Bull. Chem. Soc. Jpn.*, 2003, **76**, 309.

16 J. Liu, J.-W. Huang, B. Fu, P. Zhao, H.-C. Yu and L.-N. Li, *Spectrochim. Acta A*, 2007, **67**, 391.

17 J.X. Zhang, K.-L. Wong, W.-K. Wong, N.-K. Mak, D.W.J. Kwong and H.-L. Tam, *Org. Biomol. Chem.*, 2011, **9**, 6004.

18 M. Morone, L. Beverina, A. Abbotto, F. Silvestri, E. Collini, C. Ferrante, R. Bozio and G.A. Pagani, *Org. Lett.*, 2006, **8**, 2719.

19 H. Kon, K. Tsuge, T. Imamura, Y. Sasaki, S. Ishizaka and N. Kitamura, *Inorg. Chem.*, 2006, **45**, 6875.

20 K. Araki and H.E. Toma, *J. Photochem. Photobiol. A*, 1994, **83**, 245.

21 H.E. Toma and K. Araki, *Coord. Chem. Rev.*, 2000, **196**, 307.

22 G. Santosh and M. Ravikanth, *Inorg. Chim. Acta*, 2005, **358**, 2671.

23 K. Chichak and N.R. Branda, *Chem. Commun.*, 1999, 523.

24 E.C. Constable, A.M.W. Cargill Thompson, D.A. Tocher and M.A.M. Daniels, *New J. Chem.*, 1992, **16**, 855.

25 W. Li and Z.G. Lu, *Acta Crystallogr. E*, 2009, **65**, m1672.

26 Z. Ma, Y. Cao, Q. Li, M.F.C.G. da Silva, J.J.R.F. da Silva and A.J.L. Pombiero, *J. Inorg. Biochem.*, 2010, **104**, 704.

27 E.C. Constable, C.E. Housecroft, N.S. Murray and Z.A. Zampese, *Polyhedron*, 2013, **54**, 110.

28 D.J. Bray, J.K. Clegg, K.A. Joliffe and L.F. Lindoy, *CrystEngComm*, 2014, **16**, 6476.

29 J. E. Beves, P. Chwalisz, E. C. Constable, C. E. Housecroft, M. Neuburger, S. Schaffner and J. A. Zampese, *Inorg. Chem. Comm.* 2008, **11**, 1009.

30 R.P. Thummel, V. Hegde and Y. Jahng, *Inorg. Chem.*, 1989, **28**, 3264.

31 B. Bozic-Weber, E. C. Constable, N. Hostettler, C. E. Housecroft, R. Schmitt and E. Schönhofer, *Chem. Commun.*, 2012, **48**, 5727.

32 H. S. Chow, E. C. Constable, C.E. Housecroft, M. Neuburger and S. Schaffner, *Dalton Trans.*, 2006, 2881.

33 See for example: N. Armaroli, F. Diederich, L. Echegoyen, T. Habicher, L. Flamigni, G. Marconi and J.-F. Nierengarten, *New J. Chem.*, 1999, 77.

34 A. Klein in *Spectroelectrochemistry*, eds. W. Kaim and A. Klein, Royal Society of Chemistry, Cambridge, 2008, chapter 4, pp. 91

35 G.L. Closs and L.E. Closs, *J. Am. Chem. Soc.*, 1963, **85**, 818.

36 G.D. Dorough and F.M. Huennekens, *J. Am. Chem. Soc.*, 1952, **74**, 3974.

37 M. Gouterman, *J. Chem. Phys*. 1960, **33**, 1523.

38 J. Rodriguez, C. Kirmaier and D. Holten, *J. Am. Chem. Soc.*, 1989, **111**, 6500.

39 J.E. Monat and J.K. McCusker, *J. Am. Chem. Soc.*, 2000, **122**, 4092.

40 A.L. Smeigh, M. Creelman, R.A. Mathies and J.K. McCusker, *J. Am. Chem. Soc.*, 2008, **130**, 14105.

41 E. C. Constable, C. E. Housecroft, A. Cargill Thompson, P. Passaniti, S. Silvi, M. Maestri and A Credi, *Inorg. Chim. Acta*, 2007, **360**, 1102.

42 J.-P. Sauvage, J.-P. Collin, J.-C. Cambron, S. Guillerez, C. Coudret, V. Balzani, F. Barigelletti, L. De Cola and L. Flamigni, *Chem. Rev.*, 1994, **94**, 993.

43 V. A. Waiters, J. C. de Paula, B. Jackson, C. Nutaitis, K. Hall, J. Lind, K. Cardozo, K. Chandran, D. Raible and C. M. Phillips, *J. Phys. Chem.*, 1995, **99**, 1166